Electronic Supplementary Material (ESI) for Dalton Transactions.

Supporting information

For the paper '*Second Harmonic Generation Microscopy reveals hidden polar organization in fluoride doped MIL-53(Fe)*'

By Karen Markey, Tristan Putzeys, Patricia Horcajada, Thomas Devic, Nathalie Guillou, Michael Wubbenhorst, Stijn Vancleuvenbergen, Thierry Verbiest, Dirk De Vos, and Monique van der Veen*

X-Ray Diffractograms

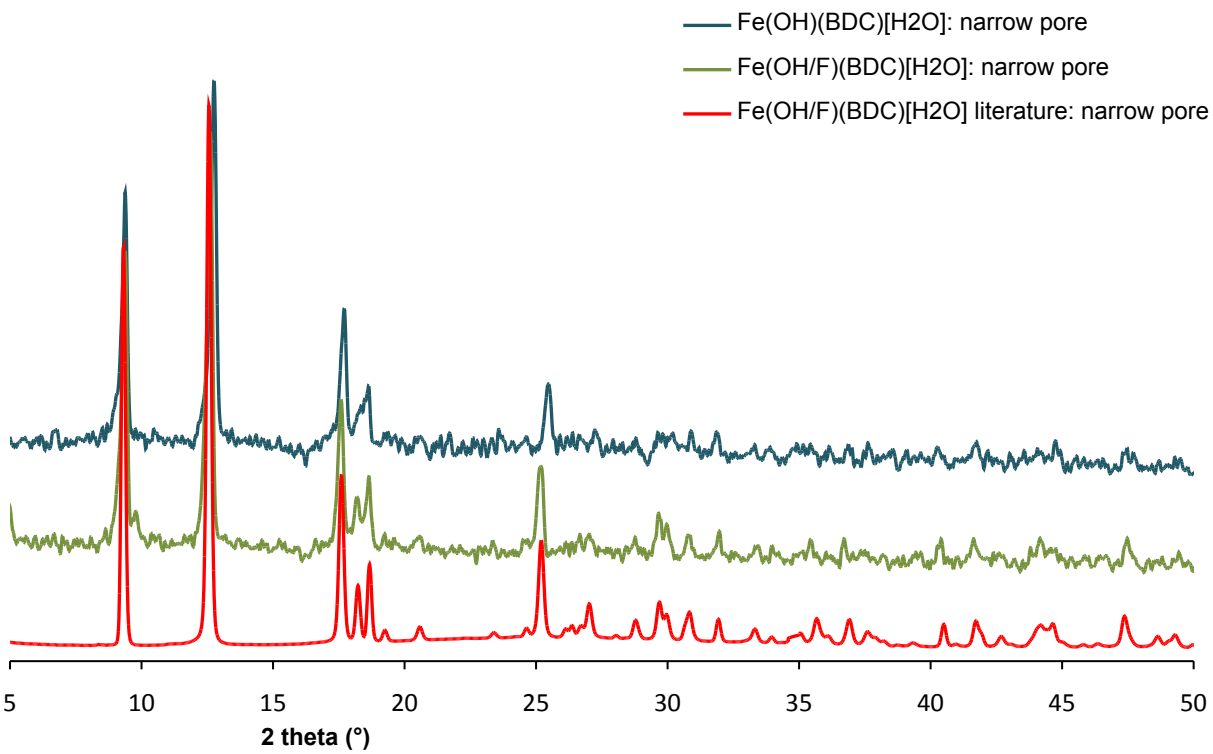

Figure S1. XRD patterns of MIL-53(Fe)·[H_2O] with and without fluoride. The high background in the patterns is due to Fe atoms in the MIL-53 structures which fluoresce due to the X-rays from the copper target that was used for the measurements. When comparing the fluorinated and non-fluorinated material small peak shifts can be observed. As reported before, the presence of fluoride in the MIL-53 framework induces some subtle structural modifications regarding guest water molecules, leading to different unit cell sizes with respect to the non-fluorinated material.[1–4] Indeed, for the "pure OH" MIL-53, a superstructure is observed leading to two types of tunnels, containing water dimers or not. The presence of fluoride makes all tunnels equivalent with one independent water molecule. The presence of fluoride clearly modifies the "host –guest" and "guest-guest" interactions.

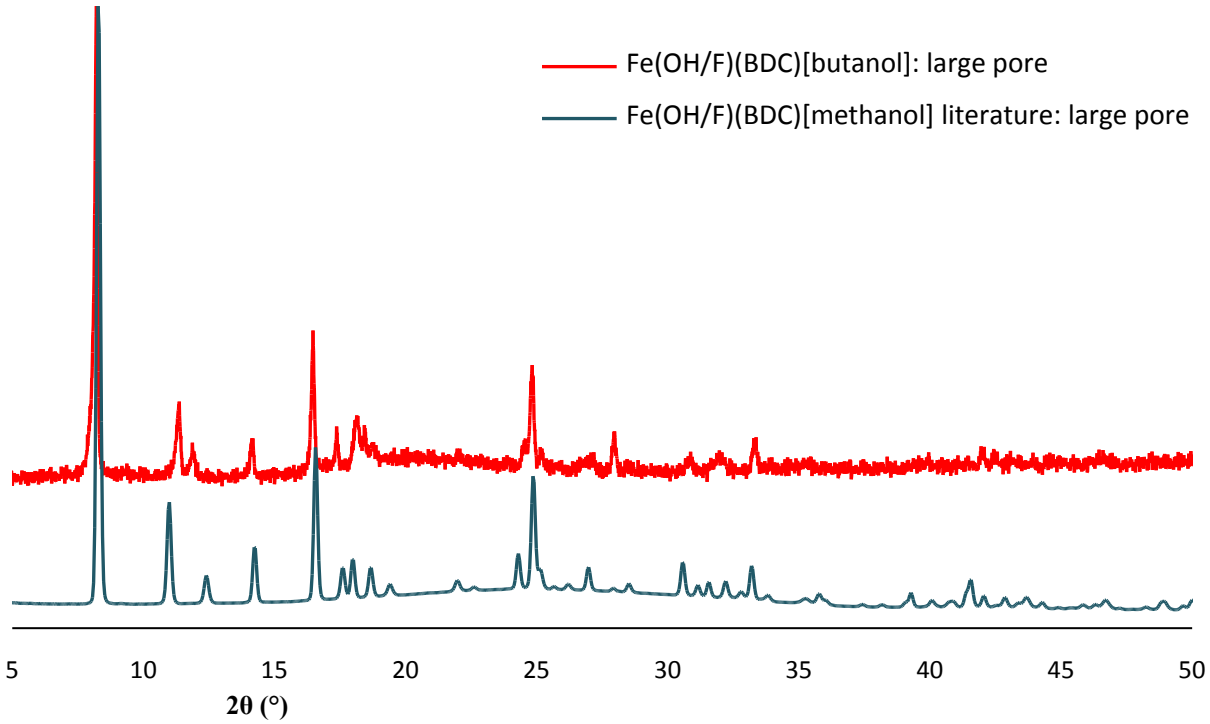

Figure S3. The capillary powder XRD pattern Fe(OH/F)(BDC)[butanol] prepared for this study resembles the pattern previously reported for Fe(OH/F)(BDC)[methanol]. The pattern with butanol in pores was not available in literature, however methanol and butanol have a similar pore opening.[5]

Thermogravimetric Analysis

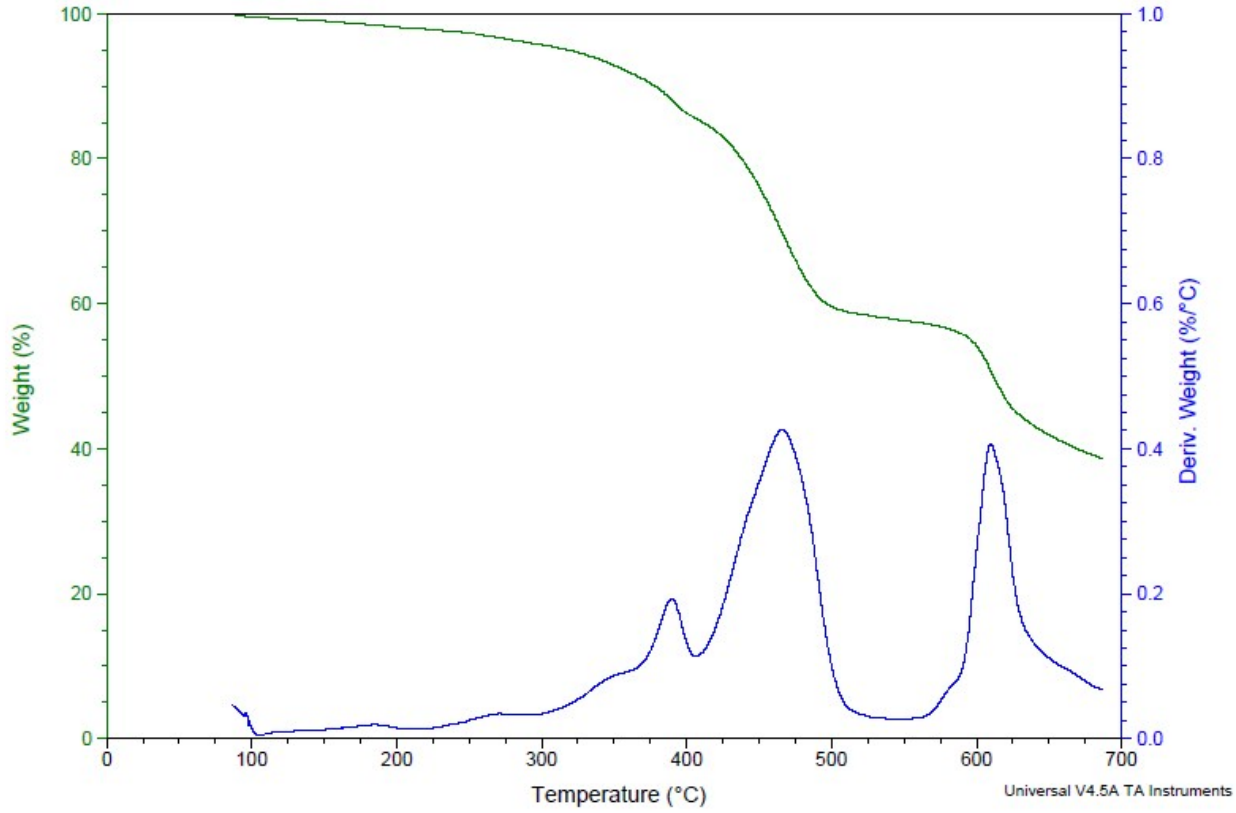

Figure S4. TGA of MIL-53 (Fe) synthesized with HF, heating 5 °C/min, N_2 flow.

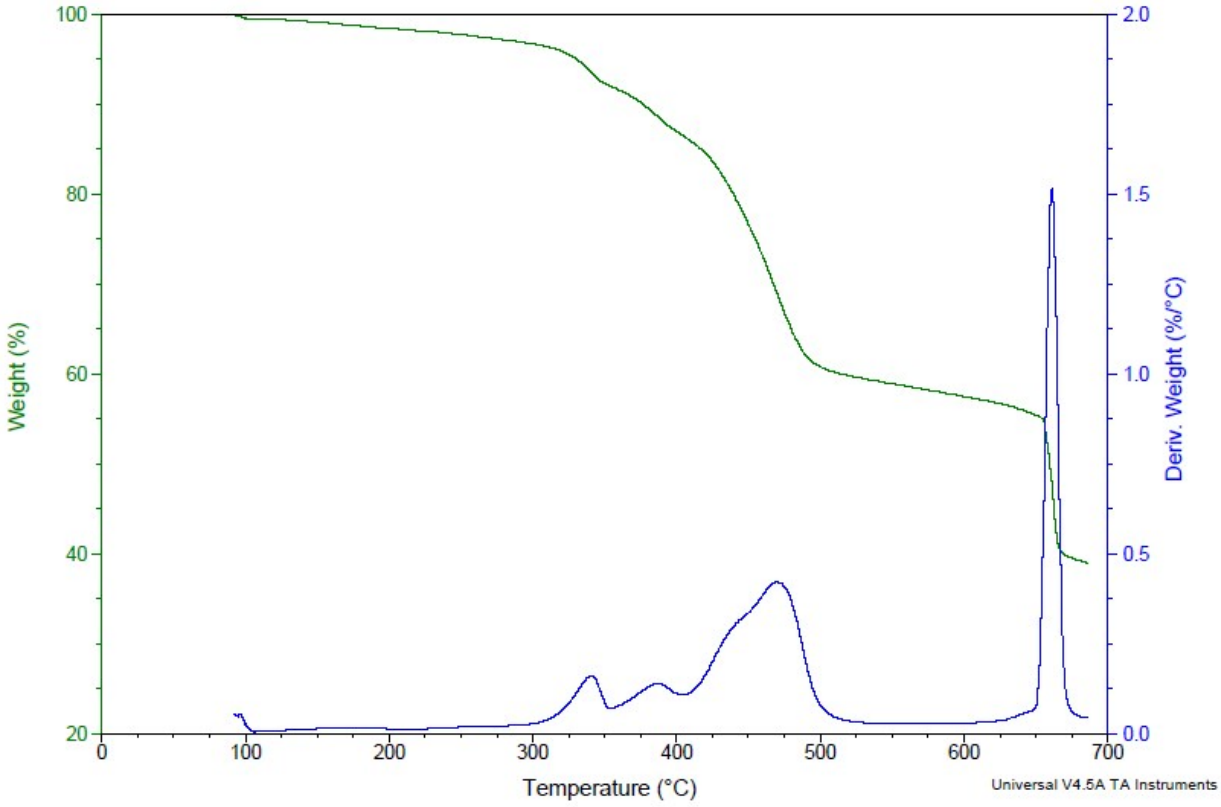

Figure S5. TGA of MIL-53 (Fe) synthesized without HF, heating 5 °C/min, N_2 flow.

Quantification of d_{eff}: the second-order nonlinear coefficient of MIL-53 (Fe)

To obtain the value for d_{eff}, the procedure as previously used by van der Veen *et al.* was followed.[6,7] Firstly, the SHG intensity of the sample was measured $(I_{2\omega,\,x})$ in an SHG wide field microscopy setup; next the SHG intensity of a reference sample was measured $(I_{2\omega,\,BBO})$. Beta barium borate (BBO) was used as a reference, 100 µm thick, cut to achieve type I phase matching and to optimize the quadratic nonlinear response (ϑ = 29.2°, φ = 90°; Eksma optics, BBO-601H). The formula for the second-order nonlinear coefficient d_{eff} was derived as follows:

$$I_{2\omega,\,x} = A\frac{< d_{eff} >^2 r^2 I_{\omega,x}^2}{n_{2\omega,x} n_{\omega,x}^2}$$

$$I_{2\omega,\,BBO} = A\frac{d_{ooe}^2 L^2 I_{\omega,BBO}^2}{n_{\theta,2\omega,BBO} n_{o,\omega,BBO}^2}$$

$$\Rightarrow \quad < d_{eff} > \; = \sqrt{\frac{I_{2\omega,x}}{I_{2\omega,BBO}} \cdot d_{ooe}^2 \cdot \frac{L^2}{r^2} \cdot \frac{I_{\omega,BBO}^2}{I_{\omega,x}^2} \cdot \frac{n_{2\omega,x} n_{\omega,x}^2}{n_{\theta,2\omega,BBO} n_{\theta,\omega,BBO}^2}}$$

With:

A = all the variables that are identical for both the sample and the BBO crystal

$I_{2\omega,\,x}$ = the SHG intensity of the MIL-53 (Fe) sample

$I_{2\omega,\,BBO}$ = intensity of the SHG light of the BBO reference, measured with a plane of polarization of linearly polarized laser light for which the SHG intensity reaches a maximum

I_{ω}= the intensity of the incident laser light, linearly polarized

r = the height of the crystallites

$n_{2\omega}$ = the refractive index at the frequency of the second-harmonic light

n_{ω} = the refractive index at the frequency of the incident laser light

The values of the refractive indices of metal-organic frameworks vary between 1.2 and 1.65 in the VIS to NIR spectral region.[8–10] Therefore, an intermediate value of 1.4 is used for both $n_{2\omega}$ and n_{ω}.

d_{ooe} = 2.01 pm/V = effective nonlinearity coefficient for type I phase-matched interaction for BBO

L = the thickness of the BBO crystal, 100 µm

$n_{\theta,2\omega,BBO}$ = extraordinary refractive index at the frequency of the SHG light, propagating at an angle ϑ with the optical axis of the crystal

$n^{2}_{o,\omega,BBO}$ = ordinary refractive index of BBO at the frequency of the incident light ω

Linearly polarized laser light was used to irradiate the sample and all the SHG signal was collected (no analyzer was positioned between the sample and the detector). To calculate the d_{eff} value for one crystal, the average over nine different orientations of linearly polarized laser light (all 10° apart) was calculated. To obtain the final $\langle d_{eff} \rangle$ value, the results were averaged over 15 different crystals.

SHG images of crystals with different guests adsorbed

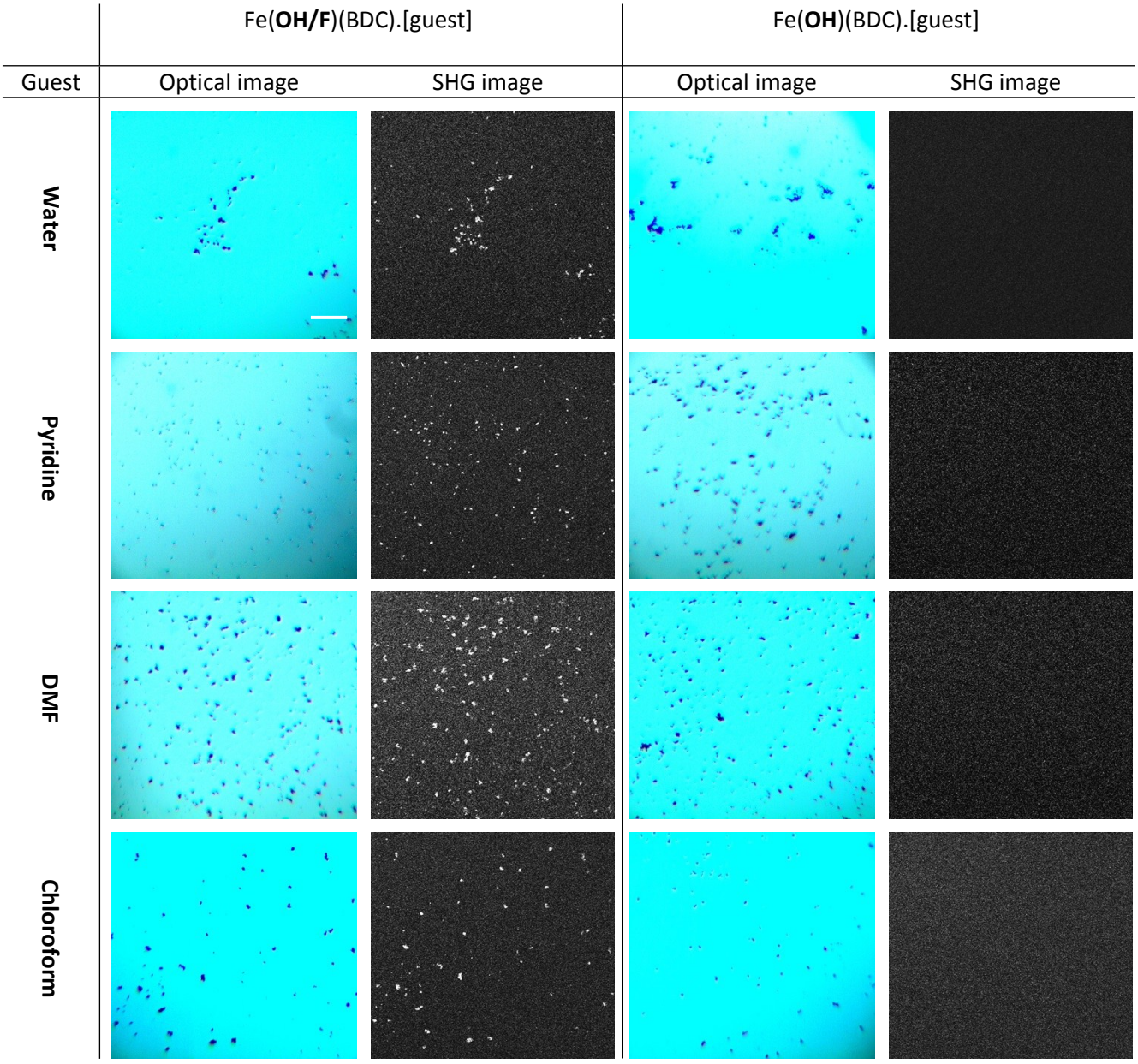

Figure S6a. (Left) Optical and SHG images of **Fe(OH/F)(BDC)** with water, pyridine, DMF and chloroform as guest molecules in the pores, clearly generating SHG signal. (Right) Optical and SHG images of **Fe(OH)(BDC)** also with water, pyridine, DMF and chloroform in the pores, with none of the crystals generating SHG signal. The scale bar on the first image is the same for all images and indicates a length of 100 μm.

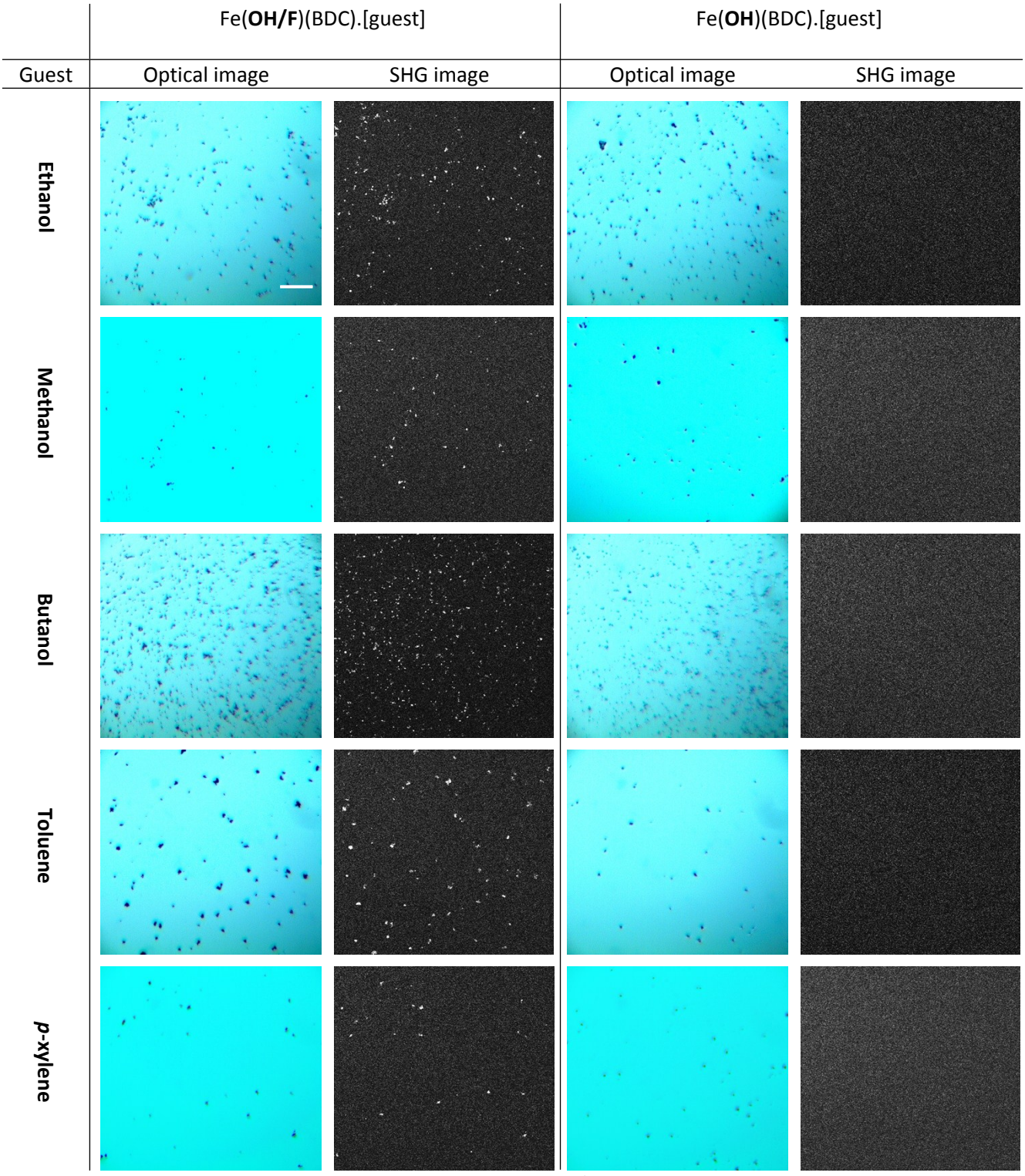

Figure S6b. On the left side: optical and SHG images of **Fe(OH/F)(BDC)** with ethanol, methanol, butanol, toluene and *p*-xylene as guest molecules in the pores, clearly generating SHG signal. On the right side: optical and SHG images of **Fe(OH)(BDC)** with ethanol, methanol, butanol and toluene in the pores, with none of the crystals generating SHG signal. The scale bar on the first image is the same for all images and indicates a length of 100 µm.

In-situ SHG measurement of heating-cooling cycle of Fe(OH/F)(BDC)·[H_2O]

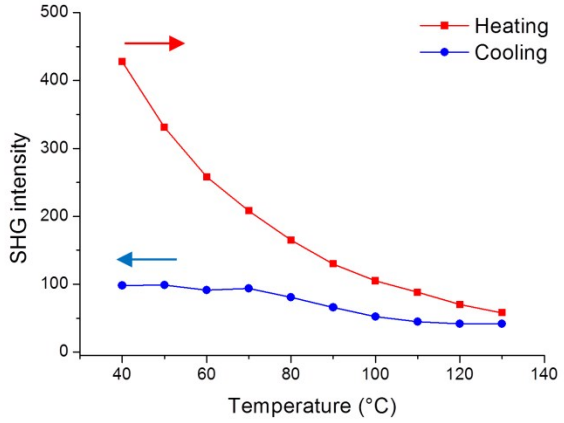

Figure S7. Changes of the SHG signal intensity during heating of an initially hydrated Fe(OH/F)(BDC)·[water] under N_2 flow, followed by cooling under N_2 flow. Heating and cooling rates were 1°C/min.

SEM of larger crystals

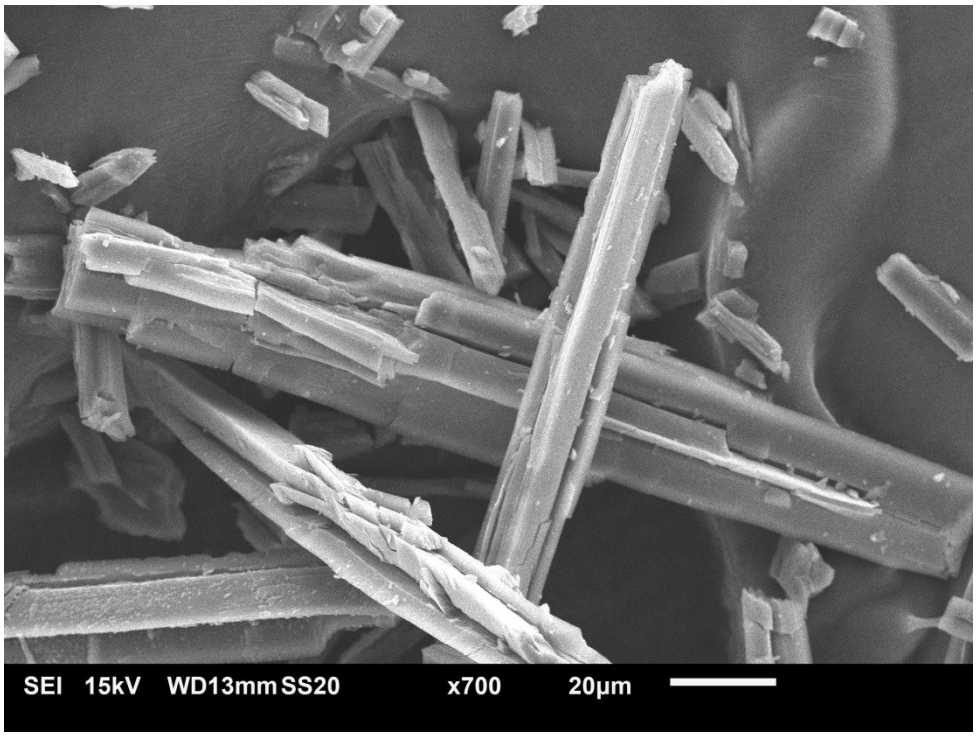

Figure S8. SEM of larger Fe(OH/F)(BDC)·[H_2O] crystals

For the symmetry probing of the non-centrosymmetric organization in MIL-53(Fe), larger crystals were grown. The crystals appear to have a rectangular shape and cracks along their long side.

Point group determination of the non-centrosymmetric organization

The symmetry of the non-centrosymmetric organization was determined via polarized nonlinear optical microscopy, using the testing procedure as described by van der Veen *et al*.[11,12] Around 30 crystals were analyzed. Figure S9 shows some results for crystals with the orientation $\theta = j\pi$. In each test the SHG intensity emitted by the crystal is recorded while the plane of the polarization of the incident laser light is rotated (α). The incident laser beam is linearly polarized and rotated along the direction of light propagation. For test 1 all the SHG light is detected. For tests 2, 3 and 4 an analyzer is positioned between the sample and the detector, therefore only the SHG light with a certain direction is detected. For test 2 the analyzer is kept fixed and the incident polarization plane is varied. In test 3 the analyzer rotates along with the plane of the incident laser light, while being parallel with it. In test 4 the analyzer also rotates along with the plane of the incident laser light, but now it is crossed with a constant difference of 90°. The patterns never reach zero intensity and are all asymmetric (no symmetry axes can be drawn in the patterns), however sometimes near symmetry is attained when the orientation of a crystal is near $\psi = j\pi$. Following the determination diagram as described by van der Veen et al. we find that this leads to possible point groups Cs, C1 and C3v, C3h, C3. When the information from XRD patterns is taken into account, Cs is the most probable point group as it belongs to the monoclinic crystal system and the space group Cc (the proposed acentric alternative refinement instead of the centric C2/c space group) falls under the Cs point group. We can therefore conclude that the point group is most likely the acentric and polar space group Cc, belonging to the Cs point group.

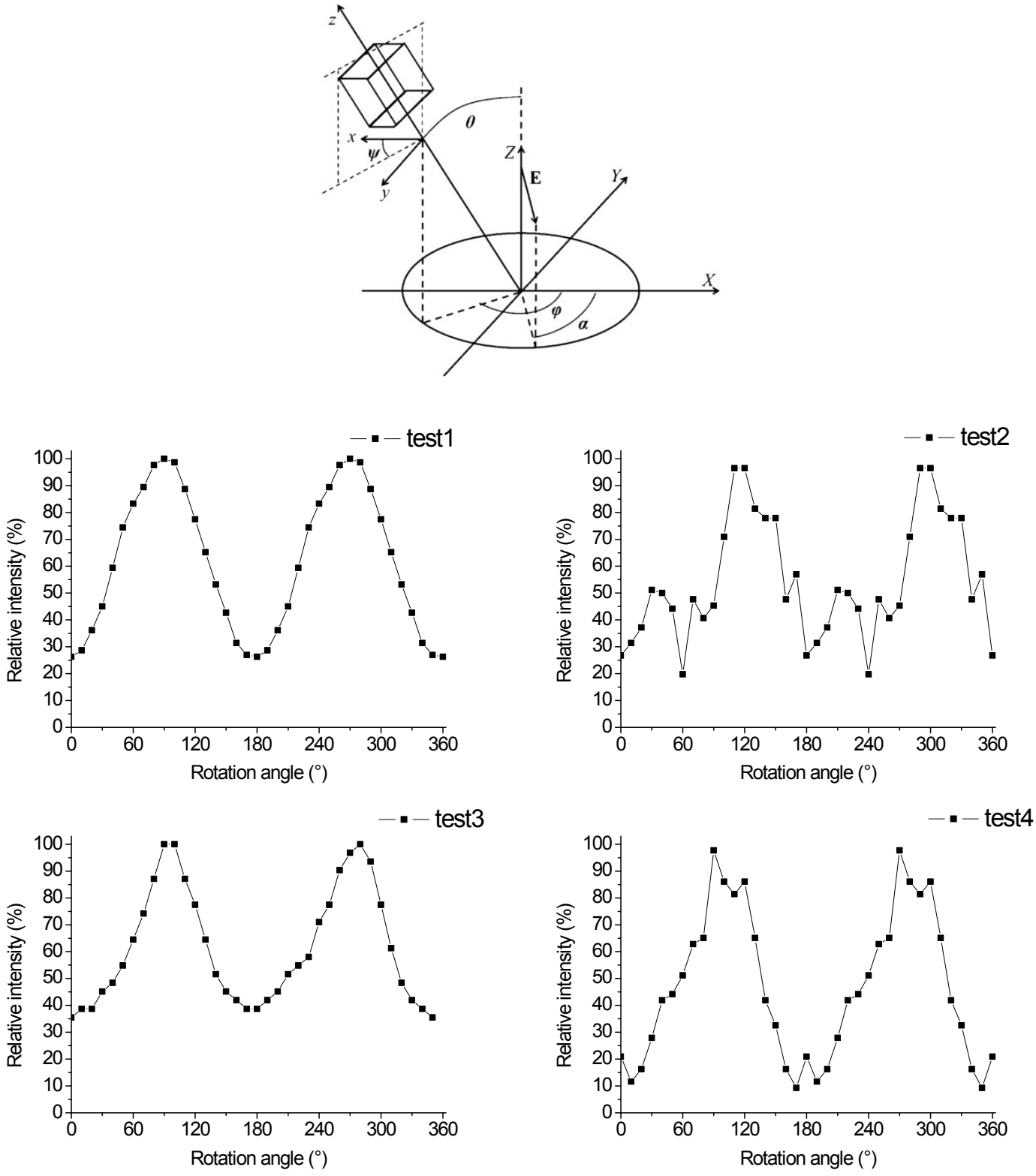

Figure S9. Point group determination patterns

Polarization map construction

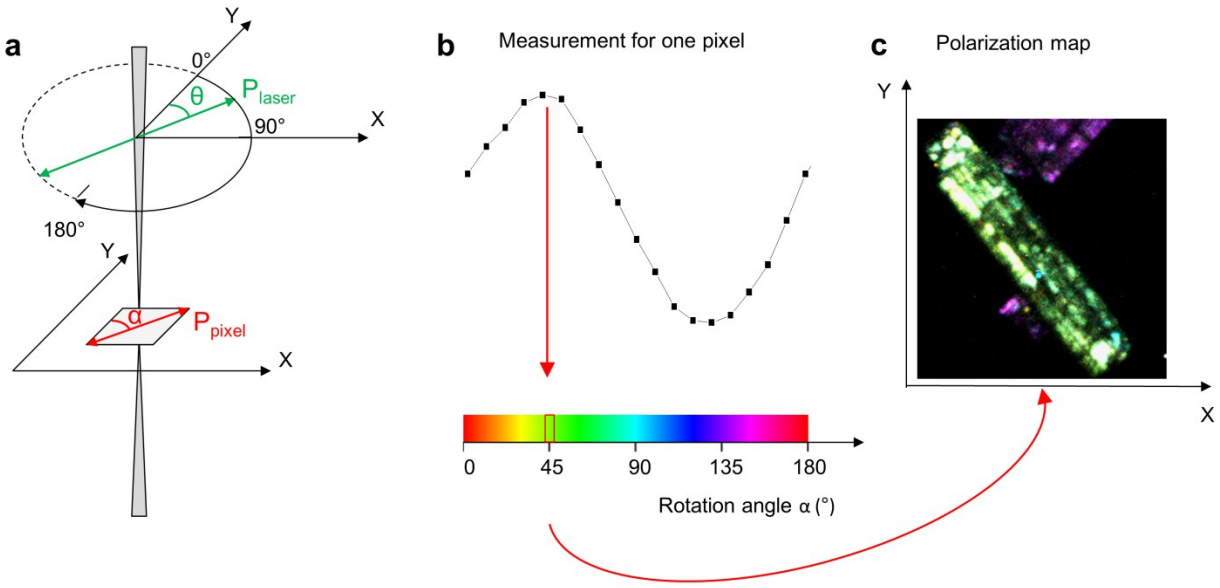

Figure S10. Schematic representation of the construction of a polarization map.

To map the polarization direction per crystal pixel in an image, the orientation α of the polarization for each pixel (P_{pixel}) in the image for which the SHG-intensity is maximal needs to be determined. When linearly polarized laser light is rotated over 180°, a maximum SHG intensity is reached when the polarization plane of the laser (P_{laser}) coincides with the direction of the local polarization of the crystal (P_{pixel}). In figure S10a the measurement method is schematically presented. To determine α, linearly polarized laser light is rotated over 180°. When the polarization sample in a pixel P_{pixel} coincides with the polarization of the laser P_{laser}, the second harmonic light generated is maximal (figure S10b), for a crystal with a polar organization. To be able to determine α, the coordinate system of the laser is aligned with that of the sample plane, as shown in part a (at angle ϑ=0° P_{laser} coincides with the Y-axis of our image plane). By assigning a color code for each value of α a polarization map such as in figure S10c is constructed, where the polarization is indicated per pixel by the color.

Bibliography

1 G. Férey, F. Millange, M. Morcrette, C. Serre, M.-L. Doublet, J.-M. Grenèche and J.-M. Tarascon, *Angew. Chem. Int. Ed. Engl.*, 2007, **46**, 3259–63.

2 C. Combelles, M. Ben Yahia, L. Pedesseau and M.-L. Doublet, *J. Phys. Chem. C*, 2010, **114**, 9518–9527.

3 N. Guillou, R. I. Walton and F. Millange, *Zeitschrift für Krist.*, 2010, **225**, 552–556.

4 R. I. Walton, A. S. Munn, N. Guillou and F. Millange, *Chem. Eur. J.*, 2011, **17**, 7069–79.

5 F. Millange, C. Serre, N. Guillou, G. Férey and R. I. Walton, *Angew. Chem. Int. Ed. Engl.*, 2008, **47**, 4100–5.

6 P. Serra-Crespo, M. A. van der Veen, E. Gobechiya, K. Houthoofd, Y. Filinchuk, C. E. A. Kirschhock, J. A. Martens, B. F. Sels, D. E. De Vos, F. Kapteijn and J. Gascon, *J. Am. Chem. Soc.*, 2012, **134**, 8314–7.

7 H. Reinsch, M. A. van der Veen, B. Gil, B. Marszalek, T. Verbiest, D. de Vos and N. Stock, *Chem. Mater.*, 2013, **25**, 17–26.

8 P. Horcajada, C. Serre, D. Grosso, C. Boissière, S. Perruchas, C. Sanchez and G. Férey, *Adv. Mater.*, 2009, **21**, 1931–1935.

9 L.-M. Yang, P. Vajeeston, P. Ravindran, H. Fjellvåg and M. Tilset, *Inorg. Chem.*, 2010, **49**, 10283–90.

10 L.-M. Yang, P. Ravindran, P. Vajeeston and M. Tilset, *Phys. Chem. Chem. Phys.*, 2012, **14**, 4713–23.

11 M. A. van der Veen, F. Vermoortele, D. E. De Vos and T. Verbiest, *Anal. Chem.*, 2012, **84**, 6386–90.

12 M. A. van der Veen, F. Vermoortele, D. E. De Vos and T. Verbiest, *Anal. Chem.*, 2012, **84**, 6378–85.